MCAT Institute
Progress Report
95-16
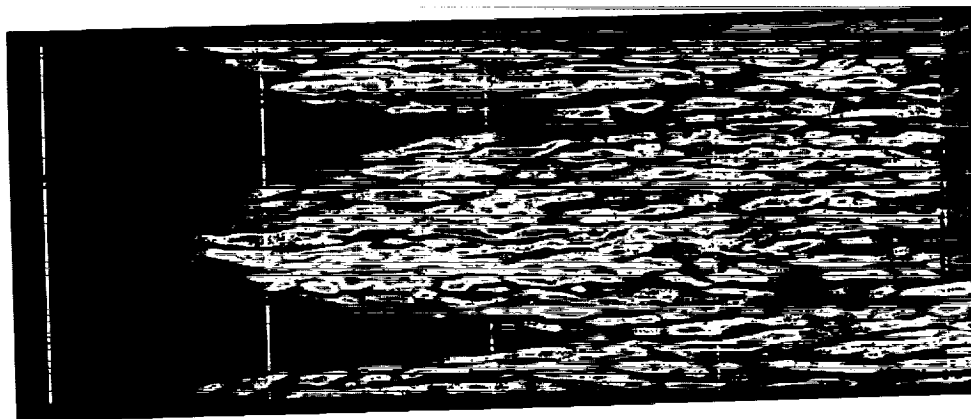
Direct Numerical Simulation of Transitional and Turbulent Flow over a Heated Flat Plate Using Finite-Difference Schemes

Nateri K. Madavan

January 1995

NCC2-755

MCAT Institute
3933 Blue Gum Drive
San Jose, CA 95127

Direct Numerical Simulation of Transitional and Turbulent Flow over a Heated Flat Plate Using Finite-Difference Schemes

Nateri K. Madavan

Abstract

This report of work performed under cooperative agreement NCC 2-755 with NASA Ames Research Center during the period August 1993 to January 1995 deals with the direct numerical simulation of transitional and turbulent flow at low Mach numbers using high-order-accurate finite-difference techniques. A computation of transition to turbulence of the spatially-evolving boundary layer on a heated flat plate in the presence of relatively high freestream turbulence was performed. The geometry and flow conditions were chosen to match earlier experiments. The development of the momentum and thermal boundary layers was documented. Velocity and temperature profiles, as well as distributions of skin friction, surface heat transfer rate, Reynolds shear stress, and turbulent heat flux were shown to compare well with experiment. The results indicate that the essential features of the transition process have been captured. The numerical method used here can be applied to complex geometries in a straightforward manner.

Introduction

Significant progress has been made in the past few years towards computing the flow fields associated with a variety of complex configurations. This can be attributed both to the increased speed and memory capabilities of computer hardware, and to improvements in computational algorithms and techniques. Complete three-dimensional solutions, both steady as well as unsteady, of the Reynolds-averaged Navier-Stokes (RANS) equations are possible on computers that are available currently.

Despite these advances, the turbulence modeling that is required in RANS computations remains a major stumbling block. The quest for an accurate and *universal* turbulence model so far has proven unsuccessful. This is because turbulence models for the RANS equations are designed to model all scales of turbulent structures. Since the larger scales are geometry- and flow-dependent, it is possible that a *universal* turbulence model accounting for all scales of motion may never be developed. In addition to turbulence modeling, the inability to accurately predict flow transition represents a second stumbling block. The solution to these problems might lie eventually in the use of techniques such as direct numerical simulations (DNS), where all pertinent scales of turbulence are computed using sufficiently fine grids that obviate the need for any modeling, and large-eddy simulations (LES), where only the smaller and more universal scales are modeled.

Despite their considerable computing requirements, a much greater reliance on such techniques is anticipated in the future as computer hardware capabilities improve.

Most of the LES and DNS research to date has been performed using spectral-based methods. Further, research efforts have dealt primarily with the temporal evolution of transition in relatively simple geometries, and have been limited to low Reynolds numbers. Such "temporal-evolution" computations are approximations to the actual spatial evolution. In recent years, finite-difference DNS techniques are being explored as an alternative to spectral-based methods. Finite-difference methods have an advantage over spectral-based methods in terms of ease of applicability to complex geometries and implementation of general boundary conditions (required for spatially-evolving flows). Recent work[1,2] has shown that the accuracy levels required for DNS and LES can be achieved by using high-order upwind-biased finite-differences. Finite difference techniques appear well-suited for conducting DNS or LES of flows in complex and more realistic configurations.

This report deals with a direct simulation of transition and turbulence in a spatially evolving boundary layer performed using high-order-accurate upwind-biased finite-difference techniques. The problem considered is the flow of a low Mach number fluid over a heated flat plate under relatively high freestream turbulence conditions. The geometry and flow conditions are chosen to match experiments[3] conducted at United Technologies Research Center and at NASA Lewis Research Center/Case Western Reserve University.[4,5,6,7,8] Our interest in the high freestream turbulence environment is two-fold. First, this is typical of several engineering applications, including gas turbine engines, that we hope to address in the future using the techniques developed here. Second, since the highly disturbed environment leads to an earlier onset of transition than in the low disturbance case, a much smaller computational domain (in the streamwise direction) is required. This in turn reduces drastically the computational effort.

Boundary layer transition in a low-disturbance environment is characterized by a well-documented sequence of events, starting with the initial amplification of two-dimensional Tollmein-Schlichting waves, followed by the formation of three-dimensional spanwise-periodic structures, development of turbulent spots, and finally culminating in random turbulent motion. The methods of linear stability theory have been used successfully to predict the Reynolds number above which small linear disturbances are amplified. However, in highly disturbed environments the presence of large disturbances may lead directly to turbulent spot formation. Morkovin[9] has used the term "bypass transition" to describe this situation where the linear instability mechanisms are bypassed by finite-amplitude nonlinear instabilities. This latter mode of transition is not very well understood.

One of the main motivations for the present work is to improve our fundamental understanding of thermal and momentum transport in transitional flows in the presence of high freestream turbulence. Such an understanding is important for many engineering applications. It is of extreme importance in improving heat transfer modeling and thermal load predictions, and determining cooling requirements for aircraft engine gas turbine blades--especially in the first stage of the high pressure turbine which is influenced largely by the combustor exit turbulence and where the flow over a large portion of the stator airfoil is typically in a transitional state. Current design

practice for turbine blading compensates for our lack of understanding by overcooling, resulting in aerodynamic cooling penalties, lowered burner and turbine mainstream mass flow rates (reduced power/efficiency), and potentially increased cooling system fabrication costs[3]. The present work eventually could impact turbine airfoil design by providing both a fundamental understanding of the flow phenomena, and information for improved modeling/computation of boundary layer transition in turbomachinery. To this end, central to this work is the creation of an extensive data base that can be used for future modeling studies, as well as validation of RANS and LES computations.

An important aspect of the present work is that we hope to shed some light on certain unexpected results that have been encountered by researchers in measuring the turbulent normal heat flux, $\overline{v't'}$, in the transitional boundary layer on a heated flat plate using three-wire probes. In the transition region, negative values were reported[6] near the wall for this correlation between the fluctuating normal velocity and the fluctuating temperature. This is an unexpected and counter-intuitive result since it implies a counter-gradient heat transfer by the fluctuations. Since the mean temperature gradient is negative, a negative value for the time-averaged $\overline{v't'}$ implies a negative eddy thermal diffusivity which would appear improbable. More recent measurements[8] in the same facility but using a different set of probes have duplicated this result, as have measurements reported by other researchers in a completely different facility.[10,11,12] Various reasons for the negative $\overline{v't'}$ correlation, including spatial resolution of the probe, wind-tunnel peculiarities, insufficient frequency response of the cold wire, thermal crosstalk between the hot and cold wires and near-wall "streaky structures", have been suggested and some of these have been subsequently disproved by measurements.[8,10] In contrast, measurements at the University of Minnesota for both flat and concave walls[13] do not exhibit negative values for the $\overline{v't'}$ correlation.

An additional aspect of the present work is the evaluation of the turbulent Prandtl number in the transition region to aid in modeling heat transfer from turbine blades. Measurements for this quantity in turbulent boundary layers have been reported by several researchers[14,15,16] but such data is lacking for transitional boundary layers.[8] This is because boundary layers in highly disturbed freestream environments undergo transition close to the leading edge, resulting in thin boundary layers that make accurate measurement somewhat difficult. The only direct measurements of the turbulent Prandtl number in transitional flows were made by Kim et al.[17] who reported measurement uncertainties higher than 20%. Other experimental efforts aimed at measuring this quantity[7,11] were beset by problems relating to the negative $\overline{v't'}$ measurement mentioned above.

The present work complements earlier DNS computations of boundary layer transition on a flat plate under adiabatic conditions.[2] A direct comparison can thus be made between the present results for a heated wall and these earlier results for an adiabatic wall. One aspect in which the present work differs from this earlier work[2] is in the treatment of the leading edge of the flat plate. Earlier, a sharp leading edge was considered; the degree to which the leading edge singularity affected the downstream flow remained a matter of conjecture. Here, the elliptical leading edge of the plate is included in the computations. This will enable leading edge receptivity studies to be performed.

Geometry and Grid System

The computational domain that was used was modeled after the configurations of prior experiments conducted at United Technologies Research Center[3] and at NASA Lewis Research Center/ Case Western Reserve University.[4,5,6,7,8] Both sets of experiments are essentially similar, differing slightly in the length of the unheated starting length and in the input heat flux. The unit Reynolds number based on inlet conditions is 50,000/inch, and the inlet Mach number, M, is 0.09. The freestream turbulence intensity in the experiments is approximately 2.6%, the onset of transition is at roughly $Re_x = 250,000$, and the flow becomes turbulent around $Re_x = 600,000$. The flat plate used in the computation has a 4:1 elliptical leading edge. As in the experiment[3], an unheated starting length of 1.7 in. (including the elliptical leading edge) is provided upstream, beyond which the flat plate is maintained at a constant heat flux of 0.075 Btu/sec.ft^2.

The computational region of interest (Fig. 1) consists of several zones. Zone 1 is an inlet region where numerically generated freestream turbulence develops. Zone 1 exchanges information with three different zones: zone 2, which covers the lower portion of the plate, zone 3, which covers the elliptical leading edge of the plate, and zone 4 which spans the region above the plate. Zone 4 represents the primary region of interest here and contains the highest grid resolution. Downstream of zone 4 is an exit region (zone 5) where the grid becomes gradually very coarse in the streamwise direction.
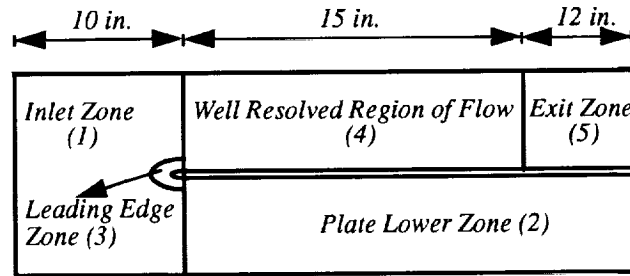
Figure 1. Flow geometry and zonal grid configuration used in the direct simulation. (Not to scale.)

The streamwise extent of the inlet region (zone 1) is 10 inches. The well-resolved region of interest on the flat plate (zone 4) spans a total of 15 in., and the exit region (zone 5) extends another 12 inches. Thus, the well-resolved region in the computation extends downstream of the plate to $Re_x = 750,000$, and includes the transition region and a portion of the turbulent region on the plate. The momentum thickness at this location is 0.031 in. (based[18] on the expression $\theta/x = 0.0142Re_x^{-1/7}$), or $Re_\theta = 1540$. The spanwise dimension of the computational region was chosen as 1.6 in., and is similar to that used in previous work.[2] The transverse extent (height) of the computational domain is 3.0 in. above and below the flat plate. (The height of the inlet region is thus 6.0 in.). Since symmetry boundary conditions are used on the upper and lower boundaries of all the zones, the simulation is in effect a channel-flow simulation, albeit a very wide channel (approximately 100 times the momentum thickness at $Re_x = 750,000$). The result-

ing acceleration of the flow is extremely small and can be neglected for purposes of comparison with experiment.

The grid system consisted of a 102 x 55 x 61 grid in zone 1, a 35 x 55 x 61 grid in zone 2, a 55 x 40 x 361 curvilinear grid in zone 3, a 1030 x 55 x 361 in zone 4, and a 97 x 55 x 361 grid in the exit zone 5. Stretched grids are used in the transverse direction with a minimum $\Delta y^+ = 1$, based on the wall shear velocity at $Re_x = 750,000$. Uniform grids are used in the spanwise direction, with $\Delta z^+ \approx 10$. For the most part, uniform grids are used in the streamwise direction in the main zone (zone 4), with $\Delta x^+ \approx 27$. Stretching in the streamwise direction is used in the initial portion of zone 4 where the flow is laminar, in zone 5 which forms the exit region, and in zone 2. The total number of grid points used is roughly 23.63 million (of which 22.38 million are in zone 4).

Numerical Method

In the present approach, the time-dependent compressible Navier-Stokes equations are solved in nonconservative form in three-dimensional Cartesian coordinates (except in the region around the leading edge where curvilinear coordinates are used). High-order accurate, upwind-biased finite-differences are used for spatial discretization and the solution is advanced in time using an iterative-implicit scheme. Upwind-biased differences are used here because they achieve higher orders of accuracy on compact stencils than fully upwind schemes. The loss of accuracy near computational boundaries where the stencil size available is smaller is thus limited. The use of the nonconservative form of the Navier-Stokes equations limits the present method to flows that are free of discontinuities (such as purely subsonic flows).

The convective terms are computed using fifth-order-accurate forward- and backward-biased finite-differences on a seven-point stencil. Viscous terms are computed using fourth-order-accurate central differences and a five-point stencil. Since we are dealing with stretched meshes, the coefficients in the difference formulas are evaluated numerically using Lagrange polynomials so as to retain high-order accuracy even on grids where the rate of change of grid spacing is not sufficiently smooth. Obtaining explicit formulas for these coefficients is a laborious task for differences with higher than second-order accuracy. Additional details regarding this procedure, and the evaluation of the convective terms and viscous terms, can be found in previous work[2].

The solution is advanced in time using an iterative-implicit approach where the fully implicit form of the equations (not the linearized implicit equations) are solved at each time step. Factorization and linearization errors are thus driven to zero at each time step. The overall method is thus fourth-order accurate in space, second-order accurate in time, and does not require the specification of any arbitrary smoothing parameters.

Boundary Conditions

The conditions imposed at the various boundaries of the computational domain are discussed here. The inlet boundary of the computational domain (left boundary of zone 1 in Fig. 1) is a subsonic inlet boundary where four quantities must be specified. The four chosen for this study are a Riemann invariant $R_1 = u + 2c/(\gamma - 1)$, the stagnation pressure, and the velocities in the y and z directions, v, w. Here u denotes the streamwise velocity and c the local speed of sound. A sec-

ond Riemann invariant, $R_2 = u-2c/(\gamma - 1)$ is extrapolated from the interior of the domain to complete the system of equations required to uniquely determine the dependent variables at the inlet. As was done in Rai and Moin,[2] small velocity perturbations are introduced at the inlet boundary. These perturbations then evolve through the domain to yield a disturbance field at the exit to the inlet region (i.e., leading edge of the plate) that closely resembles the experimental freestream turbulence. Quantities that are matched with the experiment include the turbulence intensities, the longitudinal integral length scale, and the power spectrum. Further details can be found in earlier work.[2]

The exit boundary of the domain (right boundary of zones 5 and 2) is a subsonic exit boundary where one quantity must be specified. Here the exit static pressure is specified and the remaining variables are extrapolated from the interior of the domain. The advantage of using this boundary condition in conjunction with the inlet stagnation pressure specification is that the mass flow through the domain is uniquely determined. However, this is a reflective boundary condition that reflects pressure waves back into the domain. The effects of these reflections are mitigated by gradually coarsening the grid in the exit region of the domain in the streamwise direction (by a factor of about 100).

The coarsening of the grid in the exit region serves an additional purpose. The flow across the exit boundary of the computational domain consists of an inviscid outer region (which comprises most of the area of this boundary) and the boundary layer. The static pressure from the inviscid region (in the vicinity of the boundary layer) is imposed within the boundary-layer region of the exit boundary. However, this approach is valid only when the pressure gradient normal to the wall is small (and is not the case in an unsteady turbulent boundary layer). The grid coarsening results in the unsteadiness within the boundary layer being dissipated numerically.

Symmetry boundary conditions are imposed on the upper and lower boundaries of the domain. This is done by creating temporary arrays of variables above (or below) the plane of symmetry such that the equations of motion can be integrated at grid points on the symmetry plane. Dependent variables above the plane are computed by reflection. Periodicity conditions are imposed at the spanwise boundaries of the domain.

Along the flat plate, the "no-slip" boundary condition is used together with a constant heat flux condition (or adiabatic wall in the unheated starting length region) and zero normal pressure derivative condition.

The zonal boundaries that separate the various zones are treated by using a fourth-order accurate interpolation procedure that is explicit at each iteration within a given time step, but implicit over the entire time step.[2] (The transfer of information between the inlet zone (zone 1) and the leading edge zone (zone 3) is, however, only second-order accurate.) Owing to computer memory constraints, the main zone of interest (zone 4) is divided up into several blocks and the governing equations are solved in each block in a sequential manner. This introduces additional artificial zonal boundaries. Data along several streamwise planes at either ends of each block are stored in additional arrays that are accessed when evaluating the fluxes thus maintaining the same spatial accuracy at these boundaries as at interior points. The only approximation introduced by these

artificial zonal boundaries is in the linearization, but this is driven to zero by the multiple iterations that are performed at each time step.

Results

The numerical method and boundary conditions discussed in the previous sections and the corresponding computer program were first validated by studying the growth of two-dimensional, small amplitude disturbances in flat plate flow. This investigation closely resembled that of Fasel et al.[19] A similar investigation was carried out to validate the computer code in Rai and Moin.[2] In the present investigation the inlet region, the plate leading edge, and the zonal boundaries are included and their effect on the results were documented. The results of these validation studies are not presented here, but they show excellent agreement with earlier work [2,19] and with linear theory.

Results obtained from the direct simulation of boundary layer transition on a heated flat plate are presented in this section. These results were computed by integrating the governing equations in conjunction with the boundary conditions (both natural and zonal) described in earlier sections. Three iterations were performed at each time step. The root-mean-square residual decreased by a factor of about 15 at the end of the third iteration in the main zone of interest (zone 4). Although a larger decrease in the residual is desirable, the number of iterations was restricted to three both in the interest of obtaining a solution in a reasonable amount of time and because detailed studies reported earlier[2] noted that three iterations provided adequate solution accuracy.

The results presented here were obtained in a series of stages. The initial solution was obtained on an extremely coarse grid and then interpolated onto successively finer grids. The computation on each grid was stopped when the skin-friction distribution (after spanwise averaging) showed minor changes in time and exhibited an average in time that essentially was in equilibrium.

The nondimensional time-step used in the computation was $\Delta t u_\infty / \delta^* = 0.04$, where δ^* is the boundary layer displacement thickness at the end of the well-resolved region of the plate, $Re_x = 750,000$. The maximum CFL number corresponding to this time-step is about 40.0 (the CFL number based on the mean convective velocity is approximately 4.0).

The results presented here are based on a rather small statistical sample roughly 5 milliseconds in duration. This sample size is marginally adequate for the results shown here. Much of the jitter in the results presented here is a reflection of the small sample size. More detailed analyses of the flow field such as conditional sampling or intermittency studies would require a sample that is at least ten times larger. The computer program requires about 4.5 microseconds of single-processor Cray C90 time per grid point per iteration. Approximately 300 hours of Cray C90 single-processor time was required to acquire the current sample.

Characterization of Freestream Disturbance

As described in the Boundary Conditions section, the freestream disturbance is generated by perturbing the three velocity components at the inlet of zone 1 to result in freestream disturbances at the exit to zone 1 (which is the plate leading edge) that matched the experimental conditions at

this location. The inlet perturbation velocities are obtained using a prescribed power spectrum.[3] The longitudinal integral length scale, λ_f, was taken to be 0.5 in. The intensity values at the inlet of zone 1 were iteratively modified until the intensity values at the leading edge of the plate were approximately the same as those obtained in the experiments[3] (where it is referred to as the grid No. 2 case).

Figure 2 shows the variation of u', v', w', and the freestream turbulence intensity T_{rms} in the inlet region as a function of the streamwise distance. Within a few inches from the inlet to zone 1, a decaying, nearly isotropic turbulence field is set up and the freestream turbulence intensity T_{rms} is seen to match well with the theoretical -5/7 decay law (curve marked theory in Fig. 2) for grid generated turbulence. At the exit of this region (which is the leading edge of the plate), the turbulence intensity is about 2.6%, which is the value reported in the experiments.[3] There is some variation in the intensity values for the three components. Note that the experimental data[3] also show a variation of ±15% in intensity values at the leading edge with $v' > w' > u'$.
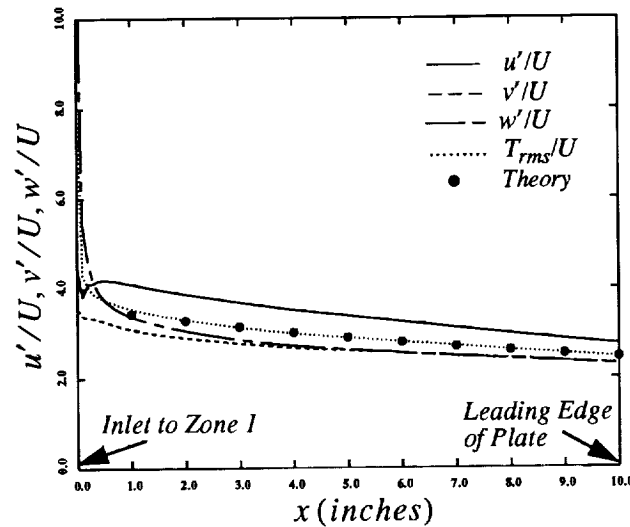
Figure 2. Variation of free-stream turbulence intensities in zone 1.

Figure 3 shows the power spectrum obtained immediately upstream of the leading edge of the flat plate for the streamwise component of the velocity. This power spectrum was computed using fast Fourier transforms in conjunction with a Hanning window.[20] The size of the window was chosen as the period of the lowest frequency perturbation introduced at the inlet to zone 1 (the lowest frequency being 24Hz). The computed spectrum roughly approximates the Von Karman spectrum. We have performed more detailed investigations that have yielded a better understanding of what is required to accurately reproduce experimentally observed freestream turbulence. This work was done under the present cooperative agreement during the period March 1992-July 1993 and is not discussed here.
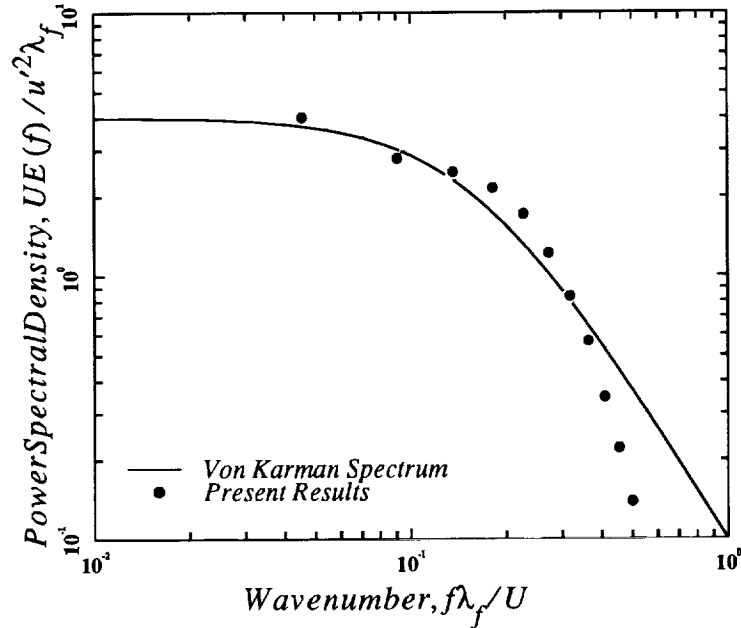
Figure 3. Computed power spectrum for the streamwise velocity component at streamwise location immediately upstream of the leading edge of the plate.

Surface Skin Friction and Heat Transfer

Figure 4 shows the computed skin friction along with experimental data,[4,6] the Blasius solution for laminar flow, and the turbulent correlation[18] for the skin friction distribution. The Blasius solution is given as:

$$C_f = 0.664Re_x^{-1/2}$$ (1)

The turbulent correlation is given as[18]:

$$C_f = 0.455/ln^2(0.06Re_x)$$ (2)

The computed data indicates onset of transition at roughly the same location as the experiment. In the transition region the computed skin friction increases rapidly and then follows the turbulent correlation. The computed rise in skin friction is much more rapid than the experimental measurement. However, there is considerable uncertainty associated with the experimental skin friction values since these are derived quantities obtained from the mean velocity profiles using the momentum integral relation. The presence of small oscillations in the computed skin friction is a reflection of the small sample size. Smoother data can be obtained by using a larger sample size.
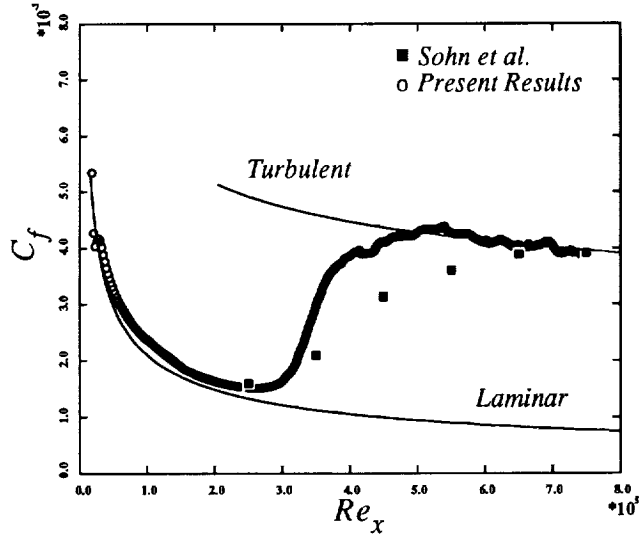
Figure 4. Computed skin-friction coefficient distribution along the length of the plate.

Figure 5 shows the computed Stanton number variation. Two sets of experimental data[3,6] are also shown in the figure, along with the expressions for laminar and turbulent boundary layers with corrections to account for the unheated starting length.[6,21] For laminar boundary layers, the Stanton number is given as:

$$St = 0.453 Pr^{-2/3} Re_x^{-1/2} (1 - (x_o/x)^{3/4})^{-1/3} \tag{3}$$

where x_o represents the unheated starting length and Pr is the Prandtl number (= 0.72). For turbulent boundary layers, the Stanton number is given as:

$$St = 0.03 Pr^{-0.4} Re_x^{-0.2} (1 - (x_o/x)^{0.9})^{-1/9} \tag{4}$$

The computed data agree well with the laminar variation. The computed onset of transition occurs slightly further downstream than in the experiments. Overall, there is reasonable agreement between the computation and experiments, with the computed results being slightly lower in the transition and turbulent flow regions. The agreement is clearly much better than for the skin friction (Fig. 4) and can be attributed largely to the higher accuracy of the Stanton number measurement. The two sets of experimental data shown in the Figure are in close agreement with each other in the transition and turbulent regions. In the laminar region, the differences between the two experimental data sets is because of slightly different unheated starting lengths. The effect of unheated starting length is much greater for laminar than for turbulent boundary layers. While the computed skin friction data seemed to agree qualitatively with the turbulent correlation beyond transition, the level of the Stanton number curve is slightly lower than the turbulent correlation. This suggests that higher grid resolution is required to match the Stanton number than required to match the skin friction.
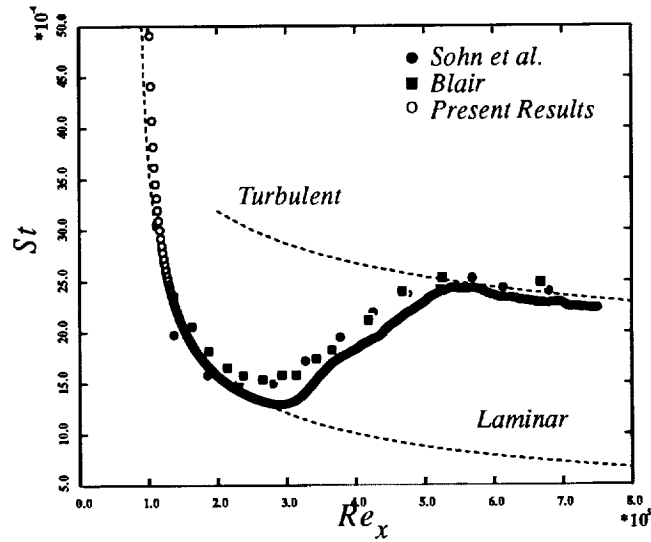
11

Figure 5. Computed Stanton number distribution
along the length of the plate.

Reynolds Analogy Factor

A plot of the Reynolds analogy factor, $2St/C_f$, is shown in Fig. 6. The Reynolds analogy factor in air for a flat plate with zero pressure gradient and a constant wall temperature boundary condition is well represented by $Pr^{-2/3}$ for both laminar and turbulent flows. However, the reference curves shown in the Figure for the laminar and turbulent regimes differ from the conventional $Pr^{-2/3}$ curve due to the effects of the uniform wall heat flux boundary condition and the unheated starting length. The curves shown were obtained by combining appropriate laminar and turbulent theoretical results.[6,21] The laminar variation plotted in the Figure is given as:

$$2St/C_f = 1.364 Pr^{-2/3} \left(1 - (x_o/x)^{3/4}\right)^{-1/3}$$ (5)

The turbulent variation is expressed as:

$$2St/C_f = 1.045 Pr^{-0.4} \left(1 - (x_o/x)^{0.9}\right)^{-1/9}$$ (6)

The computed data in the laminar and turbulent region agree quite well with the corresponding theoretical curves. The computed data in the early transition region agree with the experiment, but dip below the turbulent correlation in the late transition region before approaching the fully turbulent value. This behavior is a result of the rapid increase in skin friction that was noted in Fig. 4.
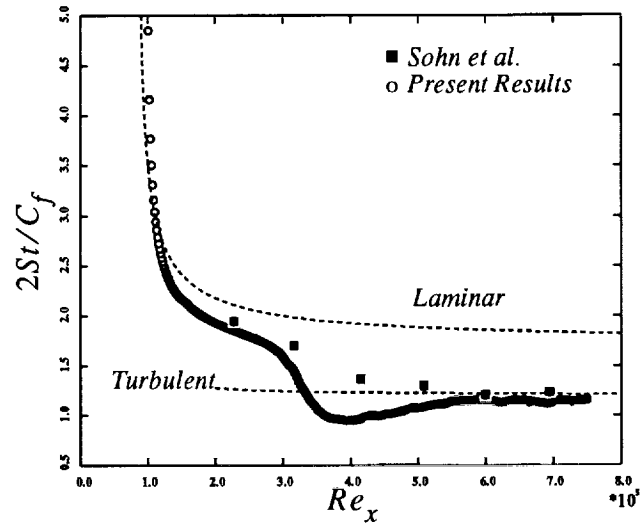
Figure 6. Computed Reynolds analogy factor distribution along the length of the plate.

Boundary Layer Thickness

The development of the boundary layer thickness in the streamwise direction is shown in Fig. 7. The local boundary layer thicknesses shown here were used to nondimensionalize the distance in the wall-normal direction in several of the figures shown later in this report. Also included in Fig. 7 are the laminar boundary layer thickness from the Blasius solution and the turbulent boundary layer thickness obtained from a momentum-integral analysis for a turbulent boundary layer.[18]
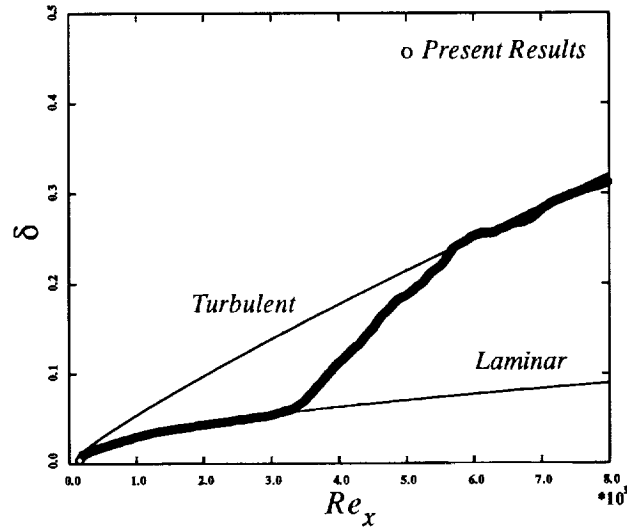
Figure 7. Development of boundary layer thickness along the length of the plate.

The laminar boundary layer thickness is obtained from the relation:

$$Re_\delta = 5.0Re_x^{1/2} \tag{7}$$

The turbulent boundary layer thickness is obtained from the relation:

$$Re_\delta = 0.14Re_x^{6/7} \tag{8}$$

The computed boundary layer thickness agrees with the laminar variation and gradually increases in the transition region to match the turbulent values.

Mean Velocity and Temperature Profiles

Figure 8 shows computed mean velocity profiles obtained at various streamwise locations. The dashed lines represent the linear relationship $u^+ = y^+$ and the logarithmic law of the wall $u^+ = 2.5lny^+ + 5.0$. The laminar or Blasius velocity profile at $Re_x = 250,000$ is also shown. The

computed velocities gradually change from laminar to the turbulent profile with increasing Re_x.
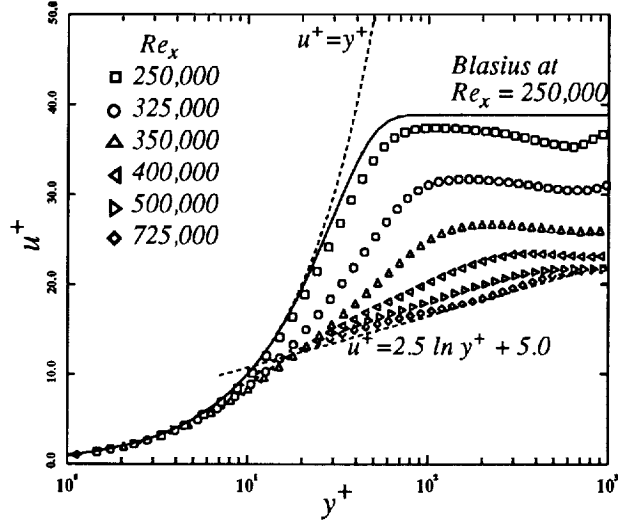
Figure 8. Mean velocity profiles at various streamwise locations, in wall units.

The changes in the velocity profiles are more rapid in the transition region than in the early turbulent region. Similar trends can be seen in the experimental data.[3,8] In the experiments, turbulent profiles are attained earlier in one experiment[8] than in the other.[3] The computed profiles indicate a transition region that lies between the two sets of experimental data. In Fig. 8, the profiles in the laminar region close to the plate leading edge show a dip in the outer portion of the boundary layer. The reasons for this are currently being investigated and appear to be related to leading edge effects. The dip gradually disappears as the streamwise distance from the leading edge of the plate increases. The computed turbulent profile at Re_x = 725,000 satisfies the law of the wall and the log-law. A significant wake region is not seen in the profile. Although the experiments clearly showed that the wake strength was diminished with increasing freestream turbulence, a small wake region was noted in the experiments at the present freestream turbulence level. The reason for this difference is not clear.

Figure 9 shows computed mean temperature profiles obtained at various streamwise locations. The dashed lines represent the equation $t^+ = Pr.y^+$ and the temperature log-law curve for fully turbulent boundary layers[6]:

$$t^+ = 13.2Pr + \frac{Pr_t}{0.41} ln \left(\frac{y^+}{13.2} \right) \tag{9}$$

where Pr is the Prandtl number (= 0.72) and Pr_t is the turbulent Prandtl number, assumed to be a constant value of 0.9. The temperature in wall units, t^+, is defined as $t^+ = (T_w - T)/t_\tau$, where t_τ is referred to as the friction temperature and is related to the wall heat flux, $\dot{q}_w$, and the friction velocity, u_τ, as $t_\tau = \dot{q}_w / \rho C_p u_\tau$. The agreement between the temperature profile in the turbulent region Re_x = 725,000 and the temperature log-law is approximately the same as shown

in Fig. 8 for the mean velocity profiles, although a wake region can be discerned in Fig. 9. A comparison of the profiles in Fig. 9 and Fig. 8 do not show any marked lag (or lead) in the development of the mean temperature compared to the mean velocity profiles. Several experimental studies [10,17,22] have noted a lag in the development of the mean temperature compared to the mean velocity profiles, but the experiments of Sohn et al.[7] show an opposite trend.
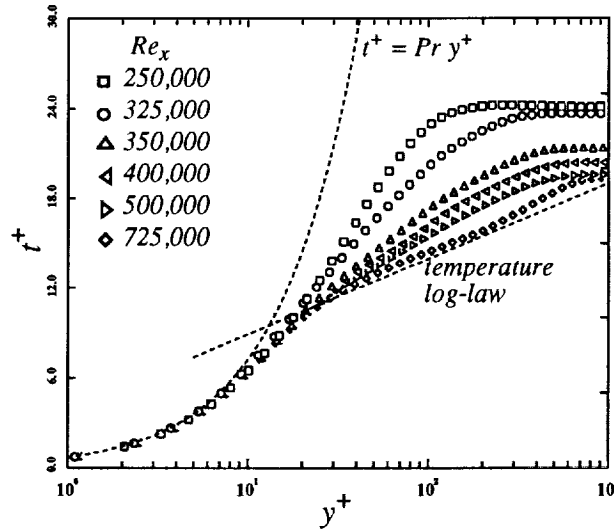

Figure 9. Mean temperature profiles at various streamwise locations, in wall units.

RMS Velocity and Temperature Profiles

Figures 10 and 11 show the evolution of the streamwise component u' of the turbulence intensity normalized by the freestream velocity at various locations along the plate. In Fig. 10 wall units are used, while in Fig. 11 outer variables are used. Both figures show that the peak value of u' increases rapidly with increasing Re_x and reaches its maximum (about 18.5% of the free-stream velocity) at about $Re_x = 400,000$ in the transitional region. Thereafter it decreases to about 15% of the free-stream velocity in the turbulent region. In terms of wall units, in the laminar and pretransitional region of the flow ($Re_x = 200,000$ and $300,000$), the peak value is located at approximately $y^+ = 27$; the peak shifts to a location $y^+ = 17$ in the transition region and remains at this location through the early turbulent region (Fig. 10). In terms of actual distance

16

from the wall, the location of the peak value can be seen moving closer to the wall with increasing Re_x in Fig. 11.
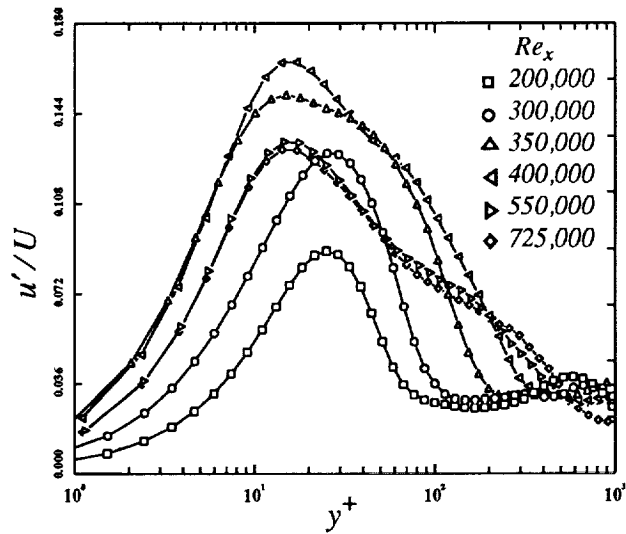

Figure 10. Streamwise component of turbulence intensity (normalized by freestream velocity) at various streamwise locations, plotted in wall coordinates.
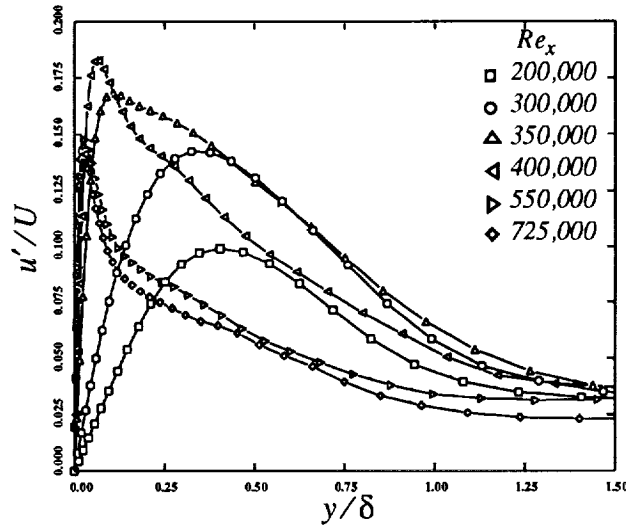

Figure 11. Streamwise component of turbulence intensity (normalized by freestream velocity) at various streamwise locations.

The general trend of the profiles in both Fig. 10 and Fig. 11 is the same as that observed experimentally.[6,4,10] However, one feature that is seen in the experiments and not in the computation is the presence of a second peak in each of the profiles in the transition region. The second peak is an artifact of the experimental technique and occurs because of the switching between laminar and

turbulent boundary layer flows as a turbulent spot goes by the hot-wire probe. The switching gives rise to a velocity fluctuation level that is higher than that obtained in either the laminar or the turbulent regions and affects the profile.[23]
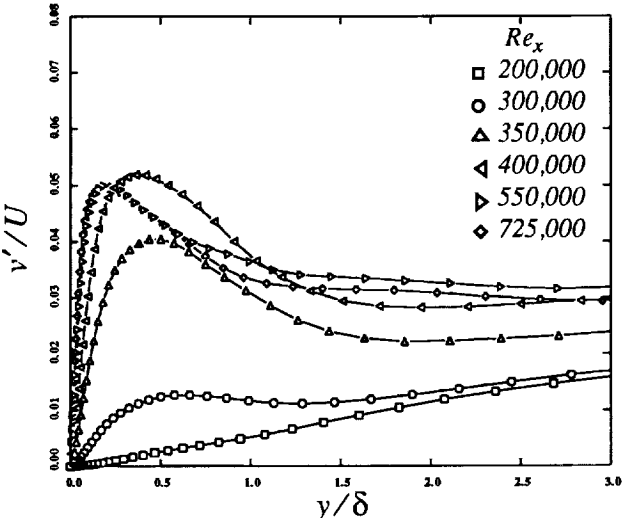
Figure 12. Normal component of turbulence intensity (normalized by freestream velocity) at various streamwise locations.
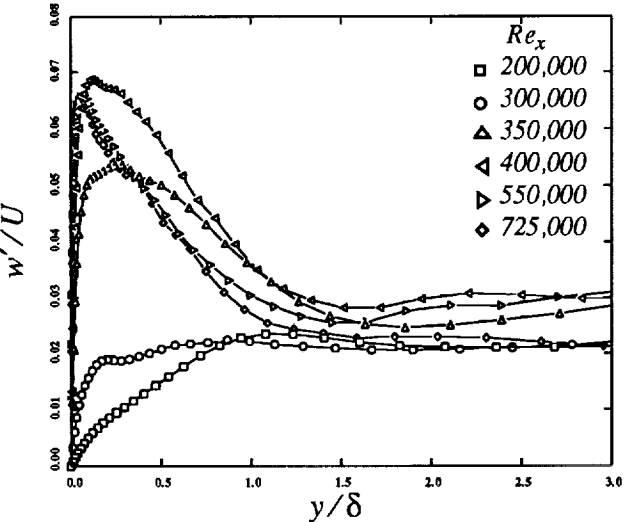

Figure 13. Spanwise component of turbulence intensity (normalized by freestream velocity) at various streamwise locations.

Figure 12 shows the normal component v' of the turbulence intensity at the same axial locations as the u' profiles shown in Fig. 11. A considerably different evolution is observed in the v' profiles than in the u' profiles. The peak value increases rapidly in the transition region with increasing Re_x to a maximum of about 5% and then maintains this value through the early turbu-

lent region. No significant decrease is observed to occur in v' once the maximum value is attained, unlike the behavior of u' which decays in the late transition/early turbulent stage. Profiles of the spanwise component w' of the turbulence intensity are shown in Fig. 13. The general trend in these profiles is similar to that seen in the v' profiles. Figure 14 shows the variation of the peak value of the three turbulent intensity components with Re_x. The trends in the peak values discussed earlier are clearly seen in this figure.
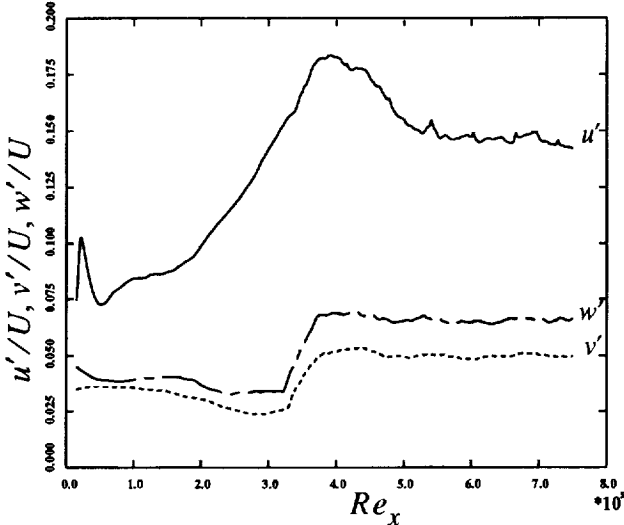
Figure 14. Variation of peak turbulence intensities with streamwise distance.

The computed turbulence intensities in the early turbulent region of the flow (at $Re_x = 725,000$) are compared to experimental data in Fig. 15. The symbols used in this Figure represent experimental data[24] obtained in a closed water channel using the LDV technique. The experimental u' and v' data were obtained at a Reynolds number based on momentum thickness, Re_θ, of 2420. The experimental w' data were obtained at $Re_\theta = 1750$. The computed data are at a streamwise location corresponding to $Re_\theta = 1350$. The free-stream turbulence level in the experiment was approximately 1.8%.

Except for u' in the region $8 \le y^+ \le 100$, the computed intensities are in good agreement with the experimental data. The nature of the discrepancy (higher u' values and slightly lower v' values) has been observed in earlier channel-flow simulations with coarse grids.[1] Additionally, computations on coarser grids in the present study clearly indicate that the major contributor to the discrepancy is the coarse grid used in the computation. The differences in the computed and experimental data for values of $y^+ \ge 500$ are mainly caused by the free-stream turbulence level in the experiment being different from that in the computation. Based on the coarse grid studies per-

19

formed here and on grid refinement studies performed earlier,[2] we expect the predicted peak value to drop to the experimental value at the next grid refinement level.
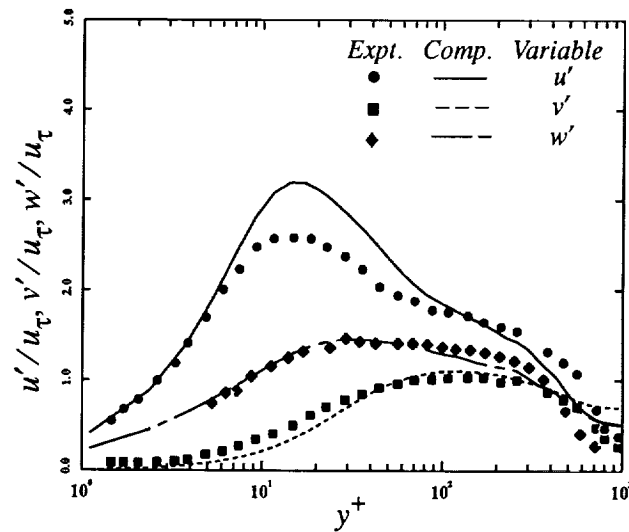

Figure 15. Turbulence intensities at streamwise location Re_x = 725,000; normalized by wall-shear velocity and plotted in wall coordinates.
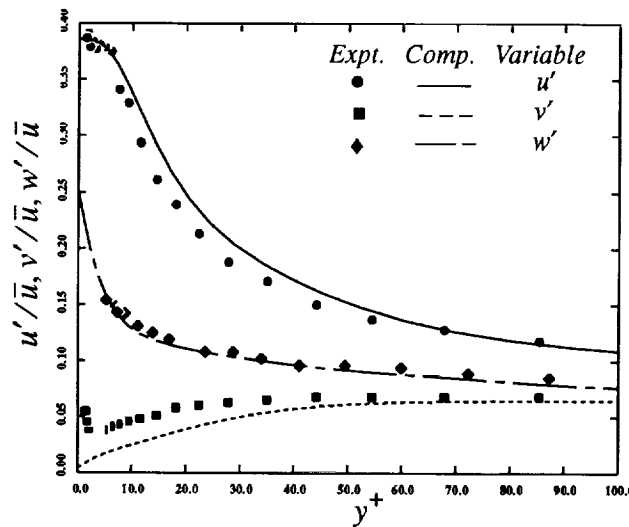

Figure 16. Turbulence intensities at streamwise location Re_x = 725,000; normalized by local mean velocity and plotted in wall coordinates.

The computed turbulence intensities normalized by the local mean streamwise velocity at the same streamwise location as in Fig. 15 (Re_x = 725,000) are shown in Fig. 16. The symbols represent the experimental data.[24] The streamwise and spanwise components agree well with the experimental data. The limiting value at the wall of the streamwise component is very nearly the same as the experimental value of 0.39. The normal component is lower than that of the experi-

mental data. It should be noted that the experimental $v'/\bar{u}$ data do not exhibit the expected linear behavior in the near-wall region; instead, they increase as the wall is approached thus indicating experimental errors.

The velocity profiles and intensity profiles presented are noted to be in good agreement with earlier computations[2] performed for an adiabatic flat plate under nearly identical flow conditions. This is to be expected, since the wall heat flux in the present study is small.
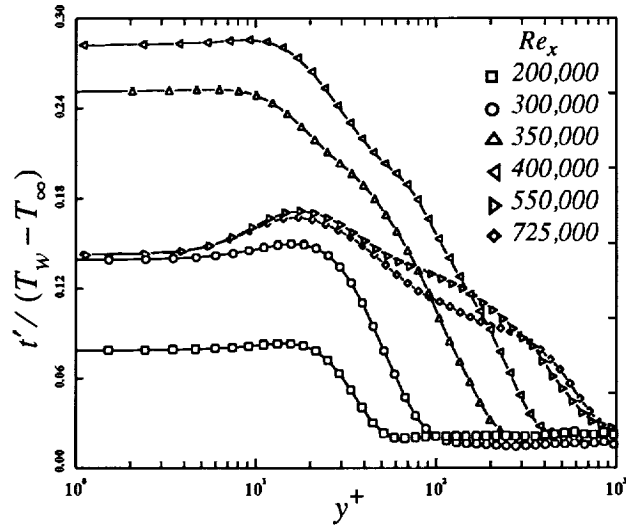
Figure 17. rms temperature fluctuations at various streamwise locations, plotted in wall coordinates.
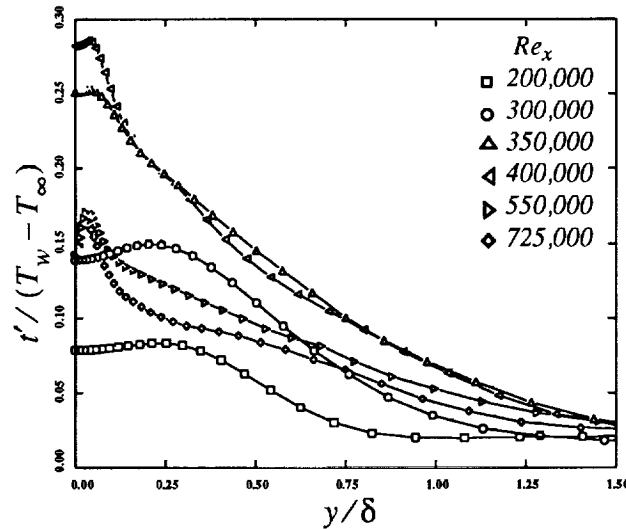
Figure 18. rms temperature fluctuations at various streamwise locations.

The rms temperature fluctuations at various streamwise locations are shown in wall units in Fig. 17 and in outer variables in Fig. 18. In both figures the temperature fluctuations are scaled by

$(T_w - T_\infty)$, where T_w denotes the local mean wall temperature. In terms of wall units, the temperature fluctuations show a plateau region up to about y^+ values of 10 - 20 and then drop off in the outer portion of the boundary layer. In the early turbulent region, the drop is more gradual than in the transitional and laminar regions. The same data when plotted in outer variables (Fig. 18) show the migration of the peak toward the wall. Both figures show the intensity of the temperature fluctuations increasing rapidly through the transition region and then decreasing in the early turbulent region.

Reynolds Shear Stress and Heat Flux Profiles

Figures 19 and 20 show Reynolds shear stress profiles at the same streamwise locations as the u' profiles shown in Fig. 11. Clearly, the peak values of these profiles follow the same trend as the u' profiles in Fig. 11. As expected, the peak values close to the leading edge are much smaller than those in the turbulent region. There is a rapid increase in peak value in the region $200,000 \le Re_x \le 400,000$. Thereafter the peak value gradually decreases to the turbulent value at $Re_x = 725,000$. Figure 20 shows a region extending from about $y^+ = 30$ to 200 in the early turbulent region where the turbulent shear stress is approximately constant.

Figure 21 compares the computed Reynolds shear stress values in the early turbulent region, $Re_x = 725,000$, with experimental data.[24] Overall there is good agreement between experiment and computation. Also, the results are very similar to earlier computations[2] for the adiabatic plate.
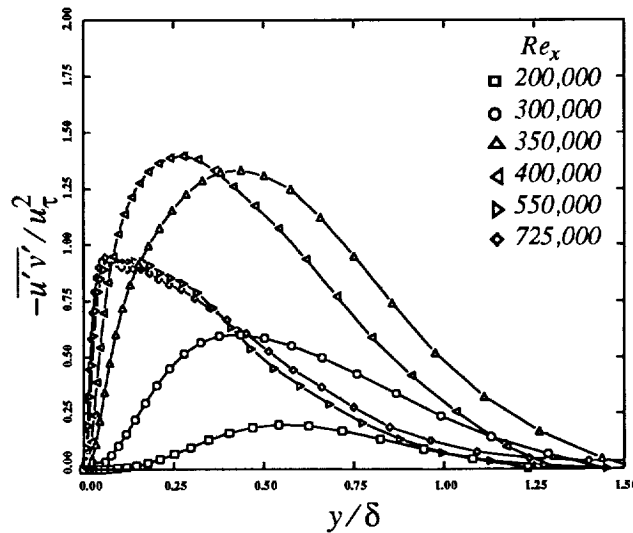

Figure 19. Reynolds shear-stress distributions at various streamwise locations; normalized by the square of the wall-shear velocity and plotted in outer variables.
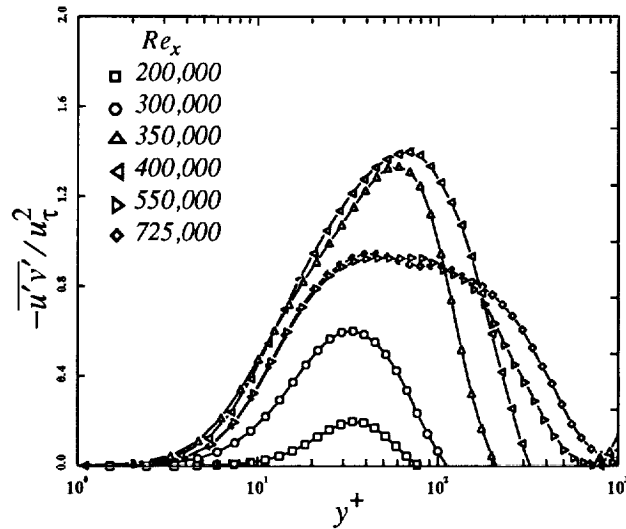
Figure 20. Reynolds shear stress distributions at various streamwise locations; normalized by the square of the wall-shear velocity and plotted in wall coordinates.
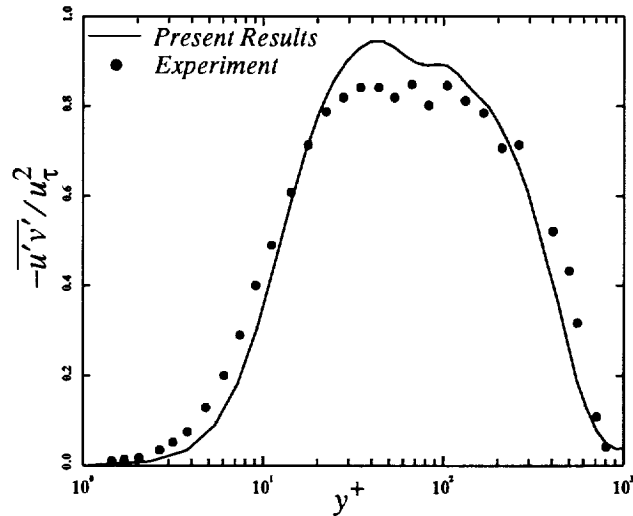

Figure 21. Reynolds shear stress distribution at the streamwise location Re_x = 725,000; normalized by the square of the wall-shear velocity and plotted in wall coordinates.

We now turn our attention to the turbulent heat flux distributions. As noted in the Introduction, one of the motivations for the present study was to shed some light on experimentally observed anomalies in the measurement of the turbulent heat flux. In particular, certain experiments showed unrealistic negative values for the turbulent heat flux near the wall in the transition region. These

unexpected experimental results still remain unresolved. Our purpose here is to determine the behavior of the turbulent heat flux through the transition region to determine if there is any basis to the experimental observations. Figures 22 and 23 show the turbulent heat flux distributions at various streamwise locations, plotted in outer and inner variables, respectively. In both the figures, the turbulent heat flux, $\overline{v't'}$, is normalized by $\dot{q}_w/\rho C_p$. There is clearly no evidence of negative values for $\overline{v't'}$ either in the transitional or in the turbulent region. Both Fig. 22 and Fig. 23 bear
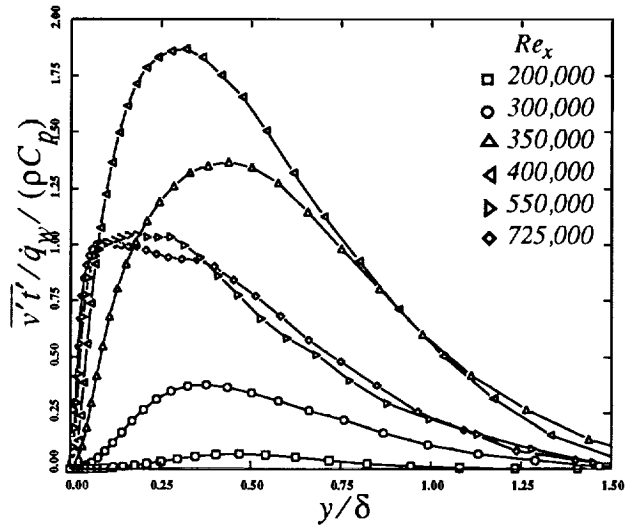

Figure 22. Turbulent heat flux distributions at various streamwise locations; normalized by $\dot{q}_w/\rho C_n$, and plotted in outer variables
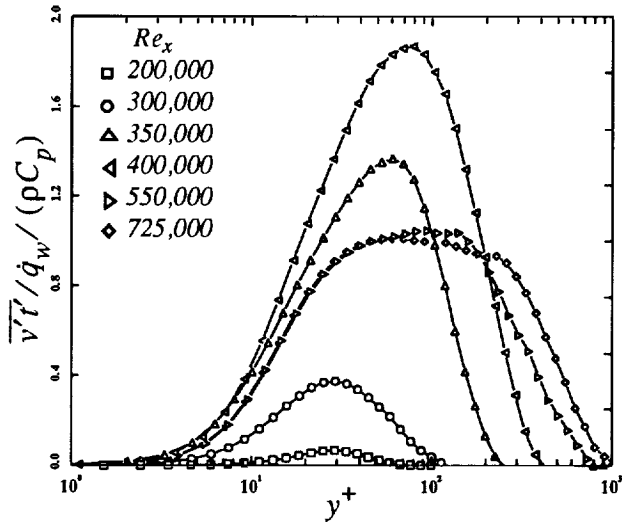

Figure 23. Turbulent heat flux distributions at various streamwise locations; normalized by $\dot{q}_w/\rho C_n$, and plotted in wall units.

24

close resemblance to the Reynolds shear stress distributions shown in Fig. 19 and Fig. 20, respectively.

Figure 24 shows the turbulent heat flux data normalized by the *rms* values of v' and t', to allow comparisons with the limited data reported in the literature for turbulent boundary layers. Figure 24 shows that in the turbulent region of the flow (Re_x = 725,000), the turbulent heat flux values range from 0.4-0.5 in the boundary layer. These values are in agreement with measurements reported in the literature for turbulent boundary layers, where values ranging from 0.42 to 0.54 have been observed.[8,14,16] Experimental data in the near-wall region is, however, lacking.
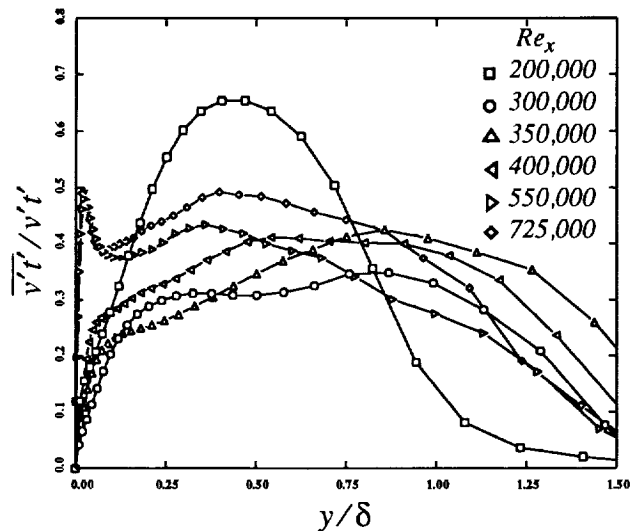

Figure 24. Turbulent heat flux distributions at various streamwise locations; normalized by the *rms* values of v' and t'.

Turbulent Prandtl Number

Figure 25 shows the computed turbulent Prandtl number distribution at various streamwise locations along the plate. At all streamwise locations, the curves are seen to rise sharply away from the wall and then drop in the outer region of the boundary layer. The location of the peak value moves closer to the wall with increasing streamwise distance. As mentioned earlier in the Introduction, to the best of our knowledge, there is only one reported set of experimental data[17] (with rather large uncertainties) for the direct measurement of Pr_t in *transitional* flows. These measurements also showed turbulent Prandtl number values (sampled on the intermittency function) substantially below unity in the near-wall region, implying that the eddy diffusivity of heat increases during transition more rapidly than does the eddy diffusivity of momentum.[17] The available experimental data for Pr_t variation in *turbulent* boundary layers show striking inconsistencies; measured data near the wall is also somewhat lacking. Some experimental results[17] show Pr_t values of unity and slightly higher everywhere in the boundary layer) while other experiments[16] show Pr_t decreasing from a peak of unity to a value of about 0.5 at the edge of the boundary layer. Outside the near-wall region, the computed results in the turbulent portion (Re_x = 725,000) seem to agree with the latter set of experiments. Note also that this behavior is similar to

the distribution suggested by Rotta.[25]. Near the wall, Pr_t drops sharply in both the transitional and turbulent region. This is in contrast to some experimental measurements[21] in turbulent boundary layers that show Pr_t rising sharply above unity near the wall.
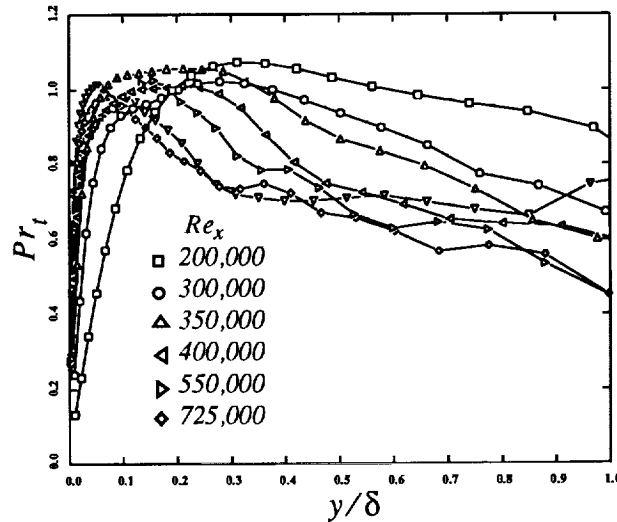

Figure 25. Computed turbulent Prandtl number distribution at various streamwise locations along the plate.

Instantaneous Flowfield Visualizations

Some limited visualizations of the instantaneous flowfield were performed using vorticity contours. More detailed visualization efforts to extract various features of the flow are currently underway.

Spanwise vorticity contours in an (x, z) plane at $y^+ = 1.0$ (based on the wall shear velocity at $Re_x = 725,000$) are shown in Fig. 26 and in Fig. 27. Figure 26 shows contours in the region $300,000 \leq Re_x \leq 500,000$. Isolated patches of vorticity are seen immersed in relatively quiescent regions. Vortical structures are seen to appear rather abruptly in the vicinity of $Re_x = 375,000$. Figure 27 shows contours in the region $500,000 \leq Re_x \leq 700,000$. The transition process is essentially completed in this region. These plots of spanwise vorticity are quite similar to earlier results[2] presented for a flat plate under adiabatic wall conditions. This is to be expected, since the freestream conditions in both cases are almost identical, and the wall heating used here is quite small.
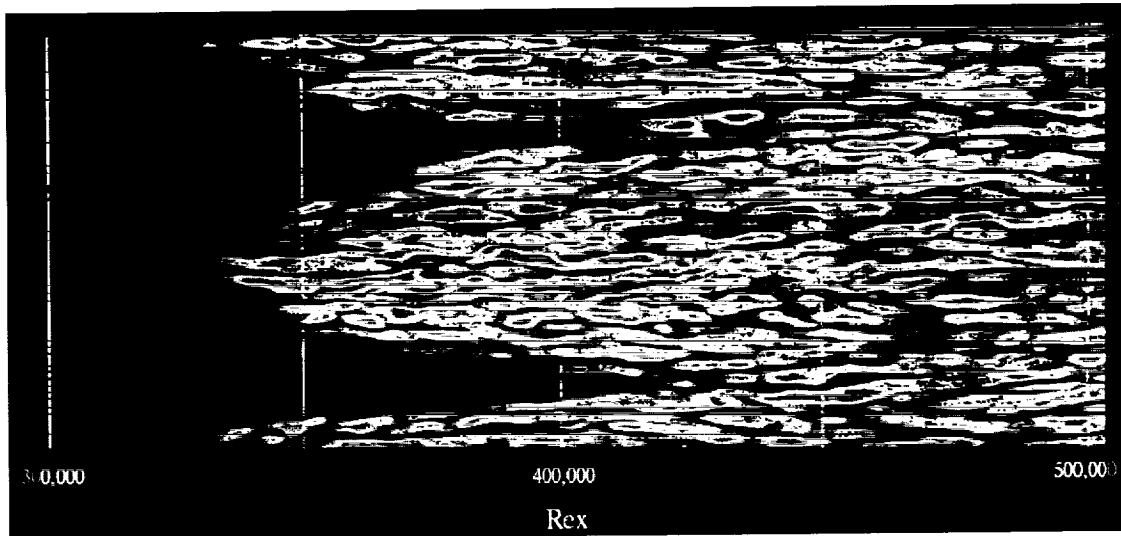
Figure 26. Spanwise vorticity contours in an (x, z) plane at $y' = 1.0$ in the region $300,000 \le Re_x \le 500,000$.
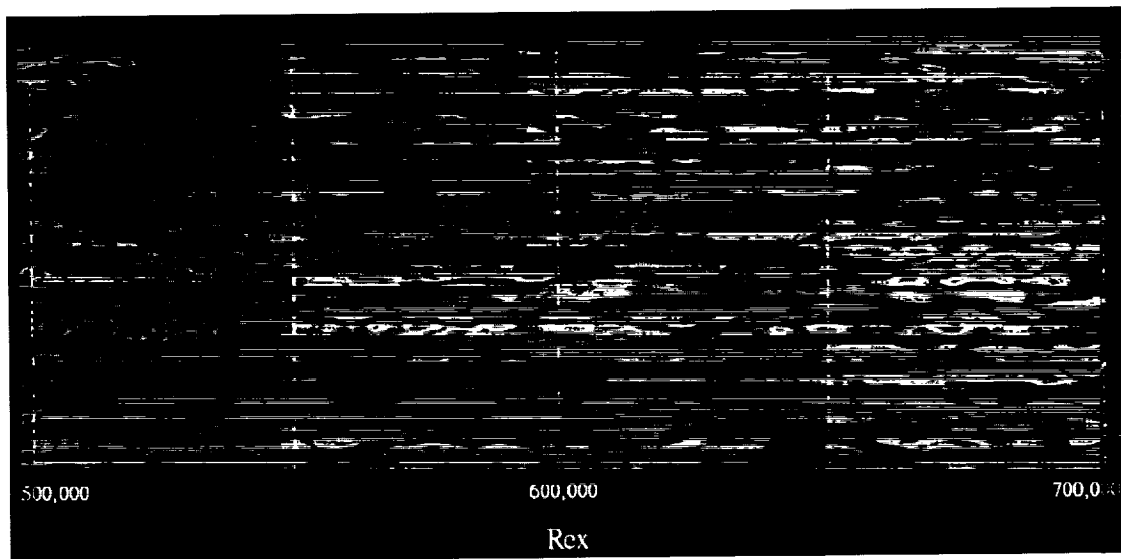

Figure 27. Spanwise vorticity contours in an (x, z) plane at $y' = 1.0$ in the region $500,000 \le Re_x \le 700,000$.

Summary

A direct simulation of transition and turbulence in a spatially evolving boundary layer on a heated flat plate is described. The simulation is performed using a high-order-accurate, upwind-biased, iterative-implicit, finite-difference algorithm. The algorithm is developed for the unsteady, compressible form of the Navier-Stokes equations. However, the simulation is performed at a low subsonic Mach number (0.09) because experimental data are available for this speed regime. This study focuses on the high-freestream disturbance case in which transition to turbulence occurs close to the leading edge, thereby substantially reducing computing requirements. A zonal approach that allows efficient and judicious distribution of the grid points is used. The zonal procedure also allowed the leading edge of the plate to be included easily in the computation. No visible degradation of solution quality was observed in the vicinity of the zonal boundaries.

A variety of information was extracted from the simulation in order to elucidate the nature of the computed transition process and provide comparisons with experimental observations. Some characteristics of the momentum and thermal boundary layers have been documented. The results indicate that the essential observed features of the transition process have been captured in the computation. Further grid refinement (factor of 3 over the grid used here) may be required to achieve a grid independent simulation. The data presented here represent only a small fraction of the information contained in the simulation database.

The results from the direct simulation show no evidence of negative values of turbulent normal heat flux in the transitional or turbulent regions. The experimentally observed negative values still remain a mystery; however, the present results indicate that it is related to the measurement technique.

In terms of future work, a computation on a refined grid is currently in progress, as are detailed flow visualization efforts. A database is being generated that can be used for developing transitional models for Reynolds-averaged Navier-Stokes computations, and for developing sub-grid scale models for large eddy simulations.

Acknowledgments

References

[1]Rai, M. M., and Moin, P., "Direct Simulations of Turbulent Flow Using Finite-Difference Schemes," Journal of Computational Physics, Vol. 96, pp. 15-53, 1991.

[2]Rai, M. M., and Moin, P., "Direct Numerical Simulation of Transition and Turbulence in a Spatially Evolving Boundary Layer," Journal of Computational Physics, Vol. 109, pp. 169-192, 1993.

[3]Blair, M. F., "Influence of Free-Stream Turbulence on Turbulent Boundary Layer Heat Transfer and Mean Profile Development, Part 1, Experimental Data," ASME Journal of Heat Transfer, Vol 105, pp. 33-40, 1983.

[4]Suder, K. L., O'Brien, J. E., and Reshotko, E., "Experimental Study of Bypass Transition in a Boundary Layer," NASA TM-100913, 1988.

[5]Sohn, K. H., O'Brien, J. E., and Reshotko, E., "Some Characteristics of Bypass Transition in a Heated Boundary Layer," NASA TM-102126, 1989.

[6]Sohn, K. H., and Reshotko, E., "Experimental Study of Boundary Layer Transition with Elevated Freestream Turbulence on a Heated Flat Plate," NASA CR-187068, 1991.

[7]Sohn, K. H., Reshotko, E. and Zaman, K. B. M. Q., "Experimental Study of Boundary Layer Transition on a Heated Flat Plate," NASA TM-103779, 1991.

[8]Sohn, K. H., Zaman, K. B. M. Q., and Reshotko, E., "Turbulent Heat Flux Measurements in a Transitional Boundary Layer," NASA TM-105623, 1992.

[9]Morkovin, M. V., "Instability, Transition to Turbulence and Predictability," AGARDAG-236, 1978.

[10]Keller, J., and Wang T., "Flow and Thermal Structures in Heated Transitional Boundary Layers With and Without Streamwise Acceleration," Final Report AFOSR-89-0324, Clemson University, June 1993.

[11]Wang, T., Keller, J., and Zhou, D., "Experimental Investigation of Reynolds Shear Stresses and Heat Fluxes in a Transitional Boundary Layer," Fundamental and Applied Heat Transfer Research for Gas Turbine Engines, ASME HTD-Vol 226, pp. 61-70, 1992.

[12]Zhou, D., and Wang, T., "Effects of Elevated Freestream Turbulence on Flow and Thermal Structures in Transitional Boundary Layers," ASME Paper 93-GT-66, presented at the International Gas Turbine and Aeroengine Congress and Exposition, Cincinnati, OH, May 24-27, 1993.

[13]Volino, R. J., and Simon, T. W., "A Review of Bypass Transition in Boundary Layers," NASA CR-187187, 1991.

[14]Chen, C. H. P, and Blackwelder, R. F., "Large-Scale Motion in a Turbulent Boundary Layer: A Study Using Temperature Contamination," Journal of Fluid Mechanics, Vol. 89, No. 1, pp. 1-31, 1978.

[15]Subramanian, C. S., and Antonia, R. A., "Effect of Reynolds Number on a Slightly Heated Turbulent Boundary Layer," International Journal of Heat and Mass Transfer, Vol. 24, pp. 1833-1846, 1981.

[16]Blair, M. F., and Bennett, J. C., "Hot-Wire Measurements of Velocity and Temperature Fluctuations in a Heated Turbulent Boundary Layer," Journal of Physics, Engineering Science and Instrumentation, Vol. 20, pp. 209-216, 1987.

[17]Kim, J., Simon, T. W., and Kestoras, M., "Fluid Mechanics and Heat Transfer Measurements in Transitional Boundary Layers Conditionally Sampled on Intermittency," ASME Journal of Turbomachinery, Vol. 116, pp. 405-416, 1994.

[18]White, F. M., "Viscous Fluid Flow," McGraw Hill, New York, 1974.

[19]Fasel, H. F., Rist, U., and Konzelmann, U., "Numerical Investigation of the Three-Dimensional Development in Boundary-Layer Transition," AIAA Journal, Vol. 28, No. 1, pp. 29-37, 1990.

[20]Choi, H., and Moin, P., "On the Space-Time Characteristics of Wall Pressure Fluctuations," Physics of Fluids A, Vol. 2, p. 1450, 1990.

[21]Kays, W. M., and Crawford, M. E., Convective Heat and Mass Transfer, 2nd Edition, McGraw-Hill, New York, 1980.

[22]Wang, T., Simon, T. W., and Buddhavarapu, J., "Heat Transfer and Fluid Mechanics Measurements in Transitional Boundary Layer Flows," ASME Journal of Turbomachinery, Vol. 109, pp. 443-450, 1987.

[23]Kim, J., and Simon, T. W., "Freestream Turbulence and Concave Curvature Effects on Heated, Transitional Boundary Layers," NASA CR-187150, 1991.

[24]Karlson, R. I., and Johansson, T. G., "LDV Measurements of Higher-Order Moments of Velocity Fluctuations in a Turbulent Boundary Layer," Laser Anemometry in Fluid Mechanics, Ladoan-Instituto Superior Tecnico, Lisbon, Portugal, 1988.

[25]Rotta, J. C., "Temperaturverteilungen in Der Turbulenten Grezschicht an Der Ebenen Platte," International Journal of Heat and Mass Transfer, Vol. 7, pp. 215-228, 1964.